Full Feedforward of Grid Voltage for Grid-Connected Inverter With *LCL* Filter to Suppress Current Distortion Due to Grid Voltage Harmonics

Xuehua Wang, Xinbo Ruan, *Senior Member, IEEE*, Shangwei Liu, and Chi K. Tse, *Fellow, IEEE*

***Abstract*—The grid-connected inverter with an *LCL* filter has the ability of attenuating the high-frequency current harmonics. However, the current distortion caused by harmonics in the grid voltage is difficult to be eliminated. Increasing the loop gain can reduce the current distortion, but this approach is compromised by the system stability requirement. Without increasing the loop gain, applying feedforward of the grid voltage can suppress the effect of grid voltage harmonics. This paper proposes the feedforward function of the grid voltage for the grid-connected inverter with an *LCL* filter. Specifically, the proposed feedforward function involves proportional, derivative, and second derivative of the grid voltage, and can be simplified according to the dominant harmonics in the grid voltage. The proposed feedforward scheme can effectively suppress the current distortion arising from the grid voltage harmonics, and the steady-state error of the injected current can be substantially reduced even if a conventional proportional and integral regulator is applied. A 6-kW experimental prototype has been tested to verify the effectiveness of the proposed feedforward scheme.**

***Index Terms*—Damping resonance, dual-loop control, feedforward, *LCL* filter, total harmonic distortions (THD).**

I. Introduction

In the past decade, the increasing demand of energy and the pressing need for reduction of greenhouse gas emission have prompted a renewed interest in the use of renewable energy, such as wind energy, microhydroenergy, and solar energy, which are rapidly increasing their share in distributed generation (DG) [1]. Unlike conventional centralized generators, these DG systems form decentralized subnetworks, providing improved power quality and reliability. However, the requirement for safe and smart operation of DG subnetworks has posed new challenges to the design of the related power electronics systems as well as the design of the subnetworks themselves (i.e., microgrids) [2]–[6]. In practice, DG subnetworks or microgrids are normally connected to the power grid through grid-connected inverters, which play an important role in ensuring high-quality power to be injected into the power grid. In the grid-connected inverter, an inductor is usually used as an interface between the inverter and the grid. However, if only an inductor is used, high-frequency switching is needed to ensure that no excessive harmonics are generated from pulsewidth modulation (PWM), but this would be accompanied by the undesirable problems of switching losses and electromagnetic interference (EMI), especially for high power applications [7].

The use of an *LCL* filter in lieu of a single inductor is an effective alternative for attenuating the current harmonics caused by PWM, since the additional capacitor branch can bypass the high-frequency harmonics. However, the frequency response of an *LCL* filter has a resonance peak, and presents zero impedance to the harmonics at the resonant frequency from the inverter or the grid. If an improper controller is used, the inverter may become unstable [8], [9].

To damp the resonance, an additional resistor can be inserted in series with the filter capacitor. This passive damping solution is very simple and highly reliable. However, the additional resistor results in power loss and weakens the attenuation ability of the *LCL* filter [10], [11]. This drawback can be overcome by employing active damping [12]–[14]. Blasko and Kaura [13] controlled the filter capacitor voltage via a lead–lag regulator to damp the resonance. The additional compensator introduces a negative resonance peak to compensate the positive resonance peak of the *LCL* filter. A similar approach based on applying feedback of the capacitor current to damp the resonance was proposed by Twining and Holmes [14]. Liserre *et al*. [15], [16] used a second-order or fourth-order digital filter to compensate the resonance peak. However, the compensation ability of the digital filter is highly dependent on the parameters of the *LCL* filter. An interesting control strategy based on the feedback of the splitting capacitor current was proposed by Shen *et al*. [11]. With this method, the injected current is not controlled directly, and the damping ability is also highly dependent upon the parameters of the *LCL* filter. Among all these active damping solutions, the solution involving feedback of the capacitor current has attracted considerable attention [14], [17].

Besides the problem associated with resonance of the *LCL* filter, the harmonics in the grid voltage is another issue in the design of grid-connected inverter. Proportional resonance (PR) regulator can provide infinite gain at the selected resonant frequency to suppress the effect of the unwanted harmonics [18]–[20]. The main disadvantage of PR regulator is that it will

Manuscript received May 25, 2010; revised August 18, 2010; accepted September 7, 2010. Date of current version December 27, 2010. This work was supported by the National Natural Science Foundation of China under Award 50837003 and Award 51007027, and the National Basic Research Program of China under Award 2009CB219706.

X. Wang, X. Ruan, and S. Liu are with the College of Electrical and Electronic Engineering, Huazhong University of Science and Technology, Wuhan 430074, China (e-mail: wang.xh@mail.hust.edu.cn; ruanxb@mail.hust.edu.cn; tsebtai@smail.hust.edu.cn).

C. K. Tse is with the College of Electrical and Electronic Engineering, Huazhong University of Science and Technology, Wuhan 430074, China, and also with the Department of Electronic and Information Engineering, The Hong Kong Polytechnic University, Hunghom, Hong Kong (e-mail: encktse@polyu.edu.hk)

Color versions of one or more of the figures in this paper are available online at http://ieeexplore.ieee.org.

Digital Object Identifier 10.1109/TPEL.2010.2077312

0885-8993/$26.00 © 2010 IEEE

reduce the system's phase margin if the harmonics to be removed is in the proximity of the crossover frequency of the loop gain [15]. Another method for suppressing current harmonics is to incorporate the variation of the grid voltage in the control through an additional feedforward path [21], [22]. The basic idea is to increase the output impedance of the grid-connected inverter, further enhancing the suppression ability. In comparison with PR regulator, this approach does not affect the phase margin. However, recent attempts in realizing this approach have only succeeded in partial feedforwarding of the grid voltage. Obviously, the suppression ability is not satisfactory.

This paper studies the feedforward scheme for grid-connected inverter with an *LCL* filter. Section II analyzes the dual-loop control strategy based on the feedback of the capacitor and the injected current, and derives a simplified mathematical model for the grid-connected inverter with an *LCL* filter based on the control strategy through a series of equivalent transformations. Based on the simplified model, Section III investigates the application of the feedforward scheme for eliminating the effect of harmonics in the grid voltage. Using the simplified block diagram, a full feedforward of the grid voltage is proposed in Section IV. The design procedure of the dual-loop controller of the proposed control strategy is presented in Section V. In order to verify the effectiveness of the proposed feedforward scheme, a 6-kW experimental prototype is built and tested. Specifically, experimental waveforms are presented in Section VI. Finally, Section VII concludes this paper.

II. System Configuration and Average Switching Model

Fig. 1(a) shows the configuration of a single-phase grid-connected inverter with an *LCL* filter. Here, the *LCL* filter is composed of L_1, C, and L_2. Fig. 1(b) shows the average switching model of the inverter with an *LCL* filter, where $v_M(s)$ is the modulating signal, and $G_{\rm inv}(s)$ is the gain of PWM inverter [11], [14], which is expressed as follows:

$$G_{\rm inv}(s) = \frac{V_{\rm in}}{V_{\rm tri}} \tag{1}$$

where $V_{\rm in}$ is the input dc voltage and $V_{\rm tri}$ is the amplitude of the carrier.

We define $Z_{L_1}(s)$, $Z_C(s)$, and $Z_{L_2}(s)$ as the impedances of L_1, C, and L_2, respectively, which are expressed as follows:

$$Z_{L_1}(s) = sL_1 \tag{2}$$

$$Z_C(s) = \frac{1}{sC} \tag{3}$$

$$Z_{L_2}(s) = sL_2. \tag{4}$$

Here, the equivalent series resistors of L_1, C, and L_2 are relatively small and can be ignored.

III. Dual-Loop Control Strategy

The primary objective of the control strategy for the grid-connected inverter is to control the current that is injected into the grid, so that it follows the grid voltage in phase and its amplitude can be regulated as required. Due to the resonance of the *LCL* filter, a single current loop is not adequate to ensure stability of the system. Thus, an inner loop incorporating feedback of the capacitor current is usually employed [14], [17], [23]. By cascading the inner loop with the outer loop, which is the injected current loop, a dual-loop control strategy is constructed. Fig. 2 shows the block diagram of the control strategy, where $i_{\rm ref}(s)$ is the injected current reference of the outer loop, $H_{i1}(s)$ and $H_{i2}(s)$ are sensor gains of the filter capacitor current and injected current, respectively, and $G_i(s)$ is the transfer function of the outer loop.

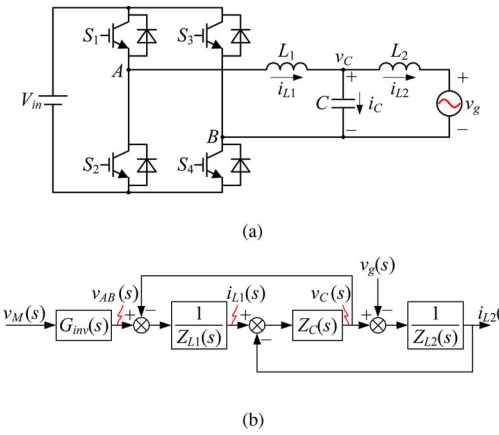

Fig. 1. Single-phase grid-connected inverter with *LCL* filter. (a) Circuit topology. (b) Block diagram of average switching model.

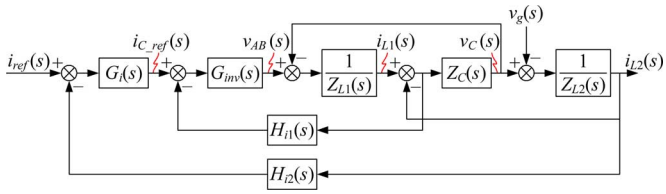

Fig. 2. Block diagram of dual-loop control strategy based on the feedback of capacitor current and injected current.

As shown in Fig. 2, the inner loop is interacting with the third-order *LCL* filter, implying that the design of the two regulating loops can be quite complicated. To simplify the design procedure, an equivalent model containing decoupled regulating loops would be desirable. A series of equivalent transformations of the system in terms of block diagrams is shown in Fig. 3, where the dash lines represent the original status, and the bold solid lines represent the destination status. First, replacing the feedback signal $v_C(s)$ with $i_C(s)$, and relocating its feedback node to the output of $G_i(s)$, an equivalent block diagram is obtained, as shown in Fig. 3(a). Second, by combining the two feedback functions of the input signal of the transfer function $Z_C(s)$, and moving the inner feedback node of $i_{L_2}(s)$ from the output of the transfer function $1/Z_{L_1}(s)$ to the output of the transfer function $G_i(s)$, the equivalent block diagram is obtained, as shown in Fig. 3(b). Third, moving the inner feedback node of $i_{L_2}(s)$ from the output of the transfer function $G_i(s)$ to the output of the transfer function $Z_C(s)$, and then, simplifying the forward path from the transfer function $G_i(s)$ to the transfer function $Z_C(s)$,

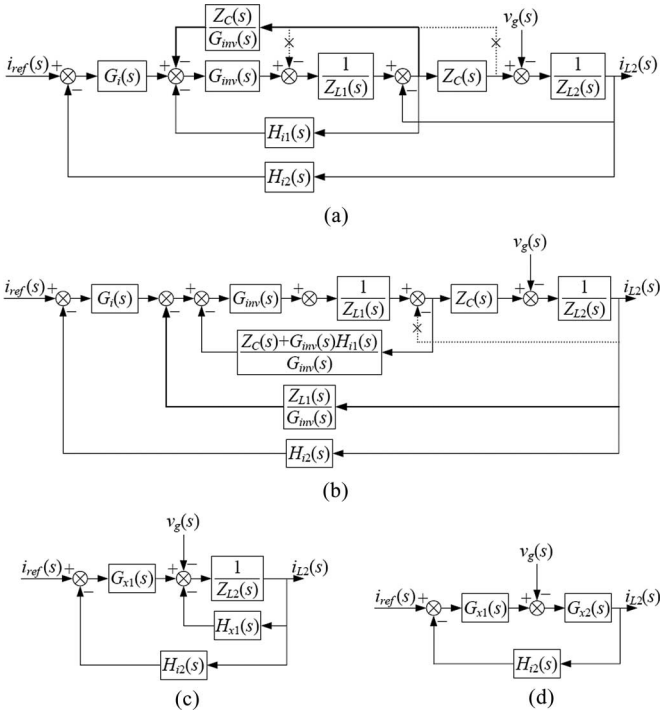

Fig. 3. Equivalent transformation of block diagram of the dual-loop control strategy.

results in the equivalent block diagram shown in Fig. 3, where

$$G_{x1} = \frac{G_i G_{\text{inv}} Z_C}{Z_{L_1} + Z_C + H_{i1} G_{\text{inv}}} \tag{5}$$

$$H_{x1} = \frac{Z_{L_1} Z_C}{Z_{L_1} + Z_C + H_{i1} G_{\text{inv}}}. \tag{6}$$

Furthermore, Fig. 3(c) can be simplified to Fig. 3(d), where

$$G_{x2} = \frac{Z_{L_1} + Z_C + H_{i1} G_{\text{inv}}}{Z_{L_1} Z_{L_2} + (Z_{L_1} + Z_{L_2}) Z_C + H_{i1} G_{\text{inv}} Z_{L_2}}. \tag{7}$$

From Fig. 3(d), the loop gain T can be obtained as follows:

$$\begin{aligned} T &= G_{x1} G_{x2} H_{i2} \\ &= \frac{G_i G_{\text{inv}} Z_C H_{i2}}{Z_{L_1} Z_{L_2} + (Z_{L_1} + Z_{L_2}) Z_C + H_{i1} G_{\text{inv}} Z_{L_2}} \end{aligned} \tag{8}$$

and the relationship between the inputs and output can be expressed as follows:

$$i_{L_2} = \frac{T}{1+T} \frac{1}{H_{i2}} i_{\text{ref}} - \frac{G_{x2}}{1+T} v_g. \tag{9}$$

From (9), we see that the steady-state error of i_{L_2} is caused by the usual static tracking error as well as variation resulting from v_g. Here, the static tracking error is a function of the current reference i_{ref}. From (7) and (9), it can be seen that if the outer loop gain G_i is large enough in magnitude, both the static tracking error and the variation resulting from v_g will be substantially reduced. However, if a conventional regulator, such as proportional–integral (PI) regulator is employed, only the static tracking error can be substantially reduced, while the variation resulting from v_g may become significant.

IV. Application of FeedForward of the Grid Voltage

Besides increasing the gain of the outer loop regulator G_i, application of feedforward of the grid voltage can also suppress the effect of v_g [22]. In (9), the function $-G_{x2}/(1+T)$ can be regarded as the admittance between v_g and i_{L_2}. If an additional path is introduced, as shown in Fig. 4(a), the effect of v_g will be eliminated. By moving the feedforward node from the output of $G_{x2}(s)$ to the output of $G_{x1}(s)$, and modifying the feedforward function as appropriate, the equivalent block diagram can be obtained, as shown in Fig. 4(b). Fig. 4(b) can be further transformed, as shown in Fig. 4(c). It can be seen from Fig. 4(c) that feedforward of v_g with the function of $1/G_{x1}(s)$ will eliminate the effect of v_g on the injected current i_{L_2}.

From Fig. 4(c), we can reconfigure the block diagram of Fig. 2, as shown in Fig. 5(a). Note that the numerator of $G_{x1}(s)$, as shown in (5), includes the function $G_i(s)$. Thus, Fig. 5(a) can be equivalently transformed into Fig. 5(b), where the feedforward component contributes to the modulation of the duty cycle.

The feedforward function in Fig. 5(b) can be expressed as follows:

$$\frac{G_i}{G_{x1}} = \frac{1}{G_{\text{inv}}} \left(1 + \frac{Z_{L_1}}{Z_C} + \frac{H_{i1} G_{\text{inv}}}{Z_C} \right). \tag{10}$$

Clearly, from (10), it can be seen that in order to eliminate the effect of v_g, three components are needed. Thus, if only $1/G_{\text{inv}}(s)$ is used, as attempted previously in [22], the result will not be very satisfactory.

Putting the three feedforward components indicated in (10) into the feedforward function in Fig. 5(b), the equivalent transformation is obtained, as shown in Fig. 6. It can be seen that one of the feedforward functions is proportional feedforward of v_g, and the other two feedforward functions are related to the impedance of the *LCL* filter. Based on (2) and (3), the other two feedforward functions are as follows:

$$\frac{H_{i1}}{Z_C} = sCH_{i1} \tag{11}$$

$$\frac{Z_{L_1}}{G_{\text{inv}} Z_C} = s^2 \frac{L_1 C}{G_{\text{inv}}} \tag{12}$$

which are the derivative and second-derivative feedforward functions of v_g, respectively.

The implementation of the proposed control strategy is shown in Fig. 7, where i_{ref} is the reference of the injected current to the grid, and H_v is the feedback coefficient of v_g. In order to ensure a high-quality current injected to the grid, i_{ref} should be controlled appropriately. In practice, the waveform of the injected current is controlled to follow a sine wave by means of table look-up using a DSP, and its phase is locked by a phase-locked loop (PLL) algorithm.

The feedforward function $G_{\text{fd}}(s)$ shown in Fig. 7 is given by

$$G_{\text{fd}} = \frac{1 + sCH_{i1} G_{\text{inv}} + s^2 L_1 C}{G_{\text{inv}} H_v}. \tag{13}$$

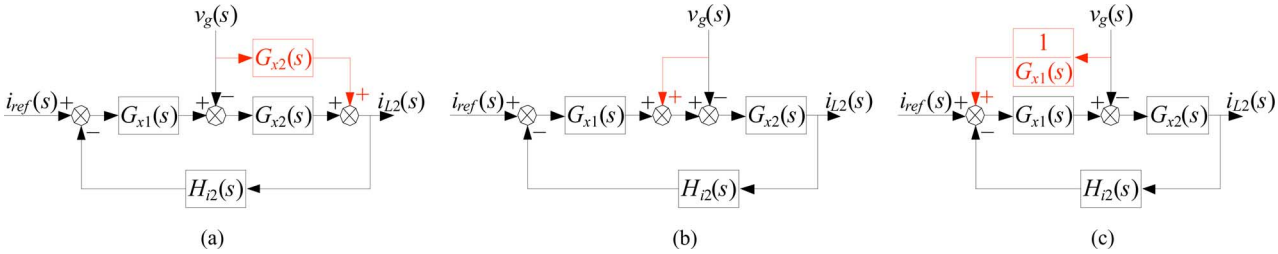

Fig. 4. Block diagram of feedforward scheme and its equivalent transforms.

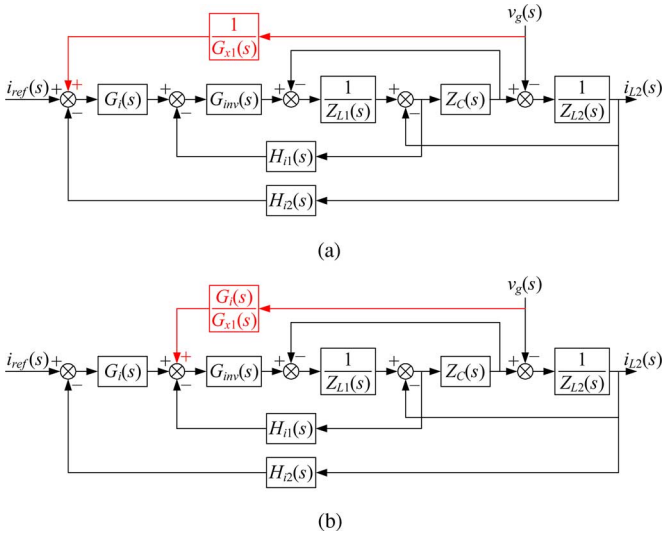

Fig. 5. Block diagrams of feedforward scheme and equivalent representations.

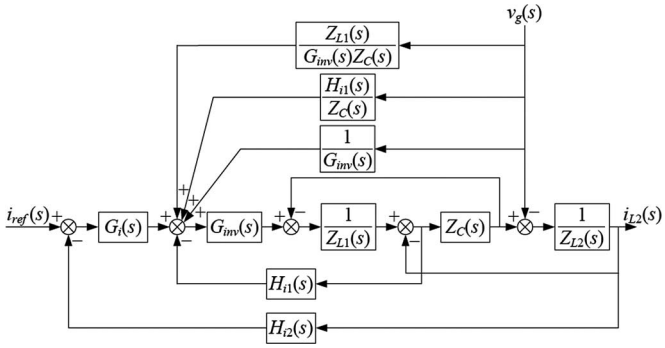

Fig. 6. Block diagrams of dual-loop control strategy with full feedforward of grid voltage.

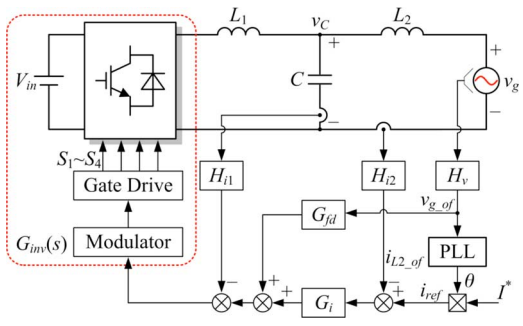

Fig. 7. Schematics diagram of the grid-connected inverter.

TABLE I
PARAMETERS OF THE PROTOTYPE

Parameter	Value	Parameter	Value
V_{in}	360 V	L_1	600 μH
V_g (rms value)	220 V	C	10 μF
f_{grid}	50 Hz	L_2	200 μH
P_o	6 kW	H_{i1}	0.075
f_s	10 kHz	H_{i2}	0.15

V. Design Procedures

A. Prototype Construction

A 6-kW prototype has been constructed to verify the proposed feedforward scheme. The parameters of the prototype are given in Table I. The controller employs carrier phase shift (CPS) sinusoidal pulsewidth modulation (SPWM).

Comparison of Figs. 2 and Fig. 6 shows that the loop gain T is not changed after the application of feedforward of v_g. Therefore, the parameters of the regulators corresponding to Figs. 2 and Fig. 6 should be the same if the stability margin is uniform. The following design is based on the dual-loop control strategy shown in Fig. 2. The inner loop will be designed first and followed by the design of the outer loop.

B. Inner Loop Design

The main objective of the inner loop is to damp the resonance. When the outer loop is uncompensated, i.e., $G_i(s)$ is 1, the loop gain expressed in (8) is as follows:

$$T_u = \frac{G_{\text{inv}} Z_C H_{i2}}{Z_{L_1} Z_{L_2} + (Z_{L_1} + Z_{L_2}) Z_C + H_{i1} G_{\text{inv}} Z_{L_2}}. \quad (14)$$

With the carrier amplitude V_{tri} is equal to 3 V, the inverter transfer function $G_{\text{inv}}(s)$ has a magnitude of 120 according to (1). In the implementation, V_{tri} is converted from a digital modulator to an analog modulator. Using the parameters in Table I, according to (14), the Bode diagrams are depicted, as shown in Fig. 8. The dashed line shows the Bode diagram without the inner loop, i.e. $H_{i1}(s)$ is 0, and it can be seen that the amplitude of the loop gain has a large resonant spike. When the inner loop is added, where $H_{i1}(s)$ is 0.075, the resonant spike is effectively damped, as shown in the solid lines.

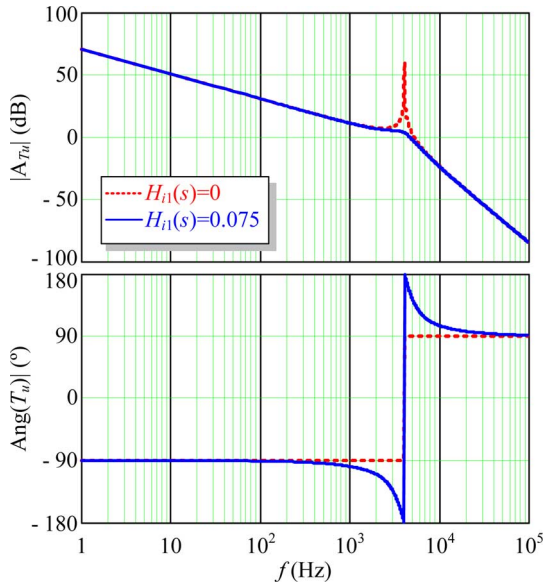

Fig. 8. Bode diagram of loop gain for inner loop design.

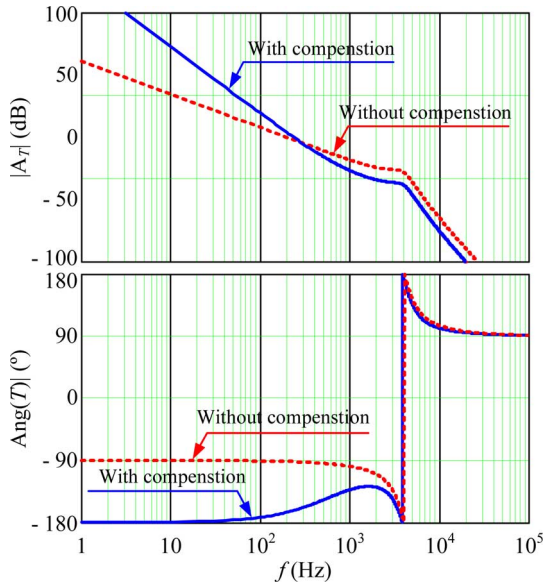

Fig. 9. Bode diagram of loop gain for outer loop design.

C. Outer Loop Design

After designing the inner loop, the parameters of the outer loop can be easily designed. Since the task of the outer loop is to reduce the steady-state error, a PI regulator can be used. When the sensor gain $H_{i2}(s)$ is set to 0.15 and the regulator $G_i(s)$ is $0.4 + 1700/s$, the Bode diagram is shown in Fig. 9. Here, the cross frequency is about 2 kHz, the amplitude margin is about 4 dB, and the phase margin is about 45°. The gain at 50 Hz is about 50 dB, which means that the disturbance can be attenuated by a factor of 0.01. Obviously, the stability margin is satisfactory and the steady-state error is acceptable.

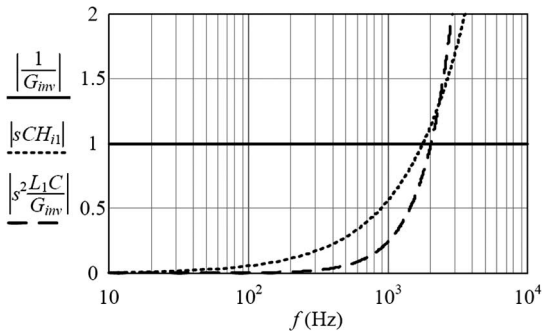

Fig. 10. Comparison of the three feedforward components.

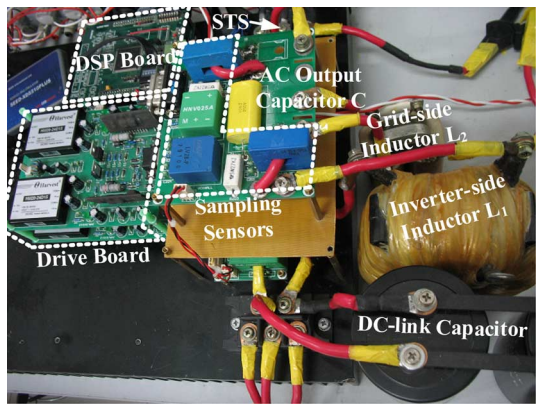

Fig. 11. Photograph of the single-phase grid-connected inverter prototype.

D. Discussion of the Three FeedForward Components

After completing the design of the dual loops, all the parameters of the grid-connected inverter are fixed, including the coefficients of the three feedforward functions. The proportional feedforward coefficient is 8.3×10^{-3}, which is the reciprocal of $G_{\rm inv}(s)$ as defined in (10). Also, as defined in (11) and (12), the derivative and second-derivative feedforward coefficients can be calculated, as shown in Fig. 10. Note that the three feedforward components are expressed in percent unit values. From Fig. 10, we can see that the derivative feedforward coefficient is an order of magnitude smaller than the proportional feedforward coefficient when v_g contains only third harmonic distortion, and that the second-derivative feedforward coefficient is also an order of magnitude smaller than the proportional feedforward coefficient when v_g contains harmonic distortion up to the 13th harmonic. This means that the second-derivative feedforward function can be omitted if v_g contains harmonic distortion within the 13th harmonic, and only the proportional feedforward coefficient is needed if v_g contains only the third harmonic.

VI. Experimental Results

A. Experimental Setup

A 6-kW prototype, as shown in Fig. 11, was constructed for verification of the full-feedforward scheme and for comparing the effectiveness of the three constituent feedforward functions. The single-phase grid-connected inverter was

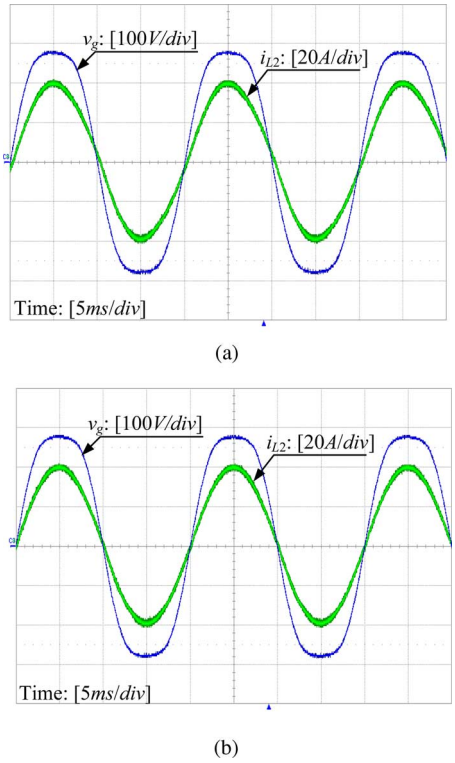

Fig. 12. Experimental waveforms of two control strategies. (a) Case I. (b) Case II.

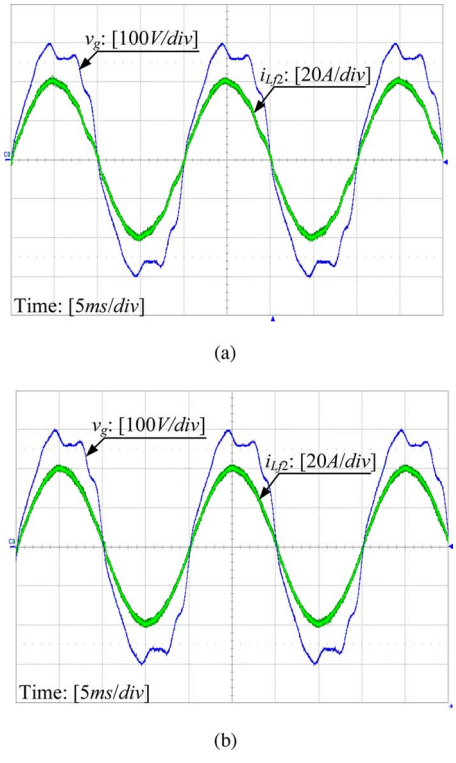

Fig. 13. Experimental waveforms of two feedforward control strategies. (a) Case II. (b) Case III.

implemented using two insulated gate bipolar transistor modules (DM2G100SH12AE). These modules are driven by M57962 L. The grid voltage v_g, which was used in the PLL, was sensed by a voltage hall (LV28-P). The capacitor current was indirectly sensed through the difference of i_{L_1} and i_{L_2}, which were measured by two current halls (LA55-P). The dual regulators were implemented by a high-speed DSP (TMS320F2812). An extended 14-bit A/D converter (MAXIM-1324ECM) was used.

In translating to the z-domain, we put $s = (1 - z^{-1})/T$ to obtain the backward difference equation for the outer loop gain, i.e.,

$$G_i(z) = k_p + \frac{k_i T_s}{1 - z^{-1}} \tag{15}$$

where k_p and k_i are the proportional and integral coefficients, and T_s is the sampling period. Likewise, the feedforward function is given in (16) as shown at the bottom of this page.

The sampling action is taken at the bottom and top of the carrier signal. In our experiment, T_s is set to 50 μs. Since the computational delay is about 2.1 μs, which is very small compared to the sampling period, the computation required by the full feedforward of v_g can be completed within a sampling period. It should be noted that a digital low-pass filter (LPF) might be needed for noise attenuation in some cases. In our case, however, the use of a LPF with corner frequency of 10 kHz has been tested and found unnecessary.

B. Results

Referring to the design procedure developed in Section V, experimental results of four cases are compared. Case I is the dual-loop strategy without feedforward of v_g, as shown in Fig. 2. Case II is the dual-loop strategy with proportional feedforward of v_g, i.e., only $1/G_{\rm inv}(s)$ is used as the feedforward function. Case III is the dual-loop strategy with proportional and derivative feedforward of v_g. Case IV is the dual-loop strategy with full feedforward of v_g, i.e., proportional, derivative, and second-derivative feedforward of v_g are all used.

We use a programmable ac source (Chroma 6590) to simulate the grid voltage. Fig. 12 shows the experimental results for Cases I and II at full-load condition. Here, the third harmonic has been injected into v_g, and the magnitude and phase of the injected harmonic is 10% and 0°, respectively, with respect to the fundamental component. It can be seen that the waveforms of i_{L_2} is distorted in Case I, and a phase difference of about 4.4° exists between i_{L_2} and v_g. It can be seen from the analysis in Section III that the phase lag is resulted from the fundamental component of v_g. Based on the parameters in Table I, the phase lag between i_{L_2} and v_g can be calculated to be 4.8°, which is

$$G_{\rm fd}(z) = \frac{\left(T_s^2 + CH_{i1}G_{\rm inv}T_s + L_1C\right) - \left(CH_{i1}G_{\rm inv}T_s + 2L_1C\right)z^{-1} + L_1Cz^{-2}}{G_{\rm inv}H_vT_s^2}. \tag{16}$$

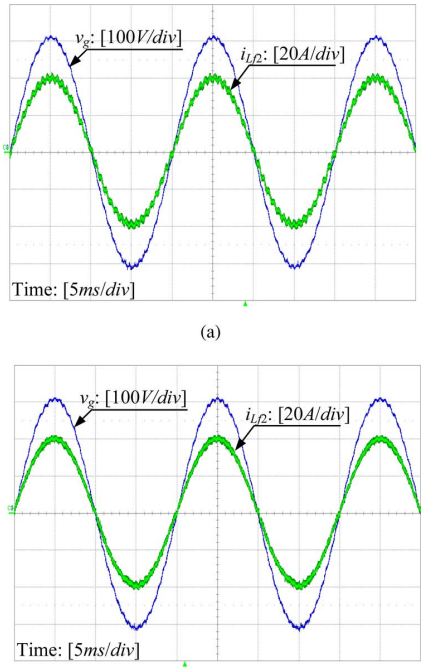

Fig. 14. Experimental waveforms of two feedforward control strategies. (a) Case III. (b) Case IV.

very close to the experimental result. For Case II, as shown in Fig. 12(b), i_{L_2} is perfectly sinusoidal, and the phase lag has been eliminated. The total harmonic distortions (THDs) of the waveforms of i_{L_2} shown in Fig. 12(a) and Fig. 12(b) are 3.21% and 1.2%, respectively. The results show that when the distortion contains only third harmonic, the proportional feedforward scheme (Case II) is effective in suppressing the distortion.

Fig. 13 shows the experimental results for Cases II and III at full-load condition. Here, the injected harmonics into v_g include the 3rd, 5h, 7th, 9th, 11th, and 13th harmonics, and the magnitudes of the injected harmonics with respect to the fundamental component of v_g are 10%, 5%, 3%, 3%, 2%, and 2%, respectively, and the corresponding phase angles are 0°, 90°, 0°, 0°, 0°, and 0°. The measured THDs of the waveforms of i_{L_2} shown in Fig. 13(a) and Fig. 13(b) are 2.61% and 1.42%, respectively. The results show that when the distortion is limited to harmonics up to the 13th harmonic, the proportional and derivative feedforward scheme (Case III) is effective in suppressing the distortion, while the proportional feedforward scheme (Case II) is inadequate.

Fig. 14 shows the experimental results for Case III and Case IV at full-load condition. Here, 33rd harmonic, with magnitude and phase of 1% and 0° with respect to the fundamental, has been injected into v_g. The measured THDs of i_{L_2} for Cases III and IV are 2.45% and 1.31%, respectively. The results show that when the distortion contains higher harmonics, the full-feedforward scheme is necessary for eliminating the distortion.

Furthermore, we conducted a test to verify the effectiveness of the proposed scheme under possible voltage dip conditions. Fig. 15 shows the experimental results for the four cases when a 40 V voltage dip occurs at the trough and crest of the voltage waveform of v_g. The THDs of i_{L_2} for the four cases are 4.61%, 5.42%, 3.26%, and 2.24%, respectively. The results show that the full-feedforward scheme can effectively suppress the current distortion even v_g experiences a voltage dip.

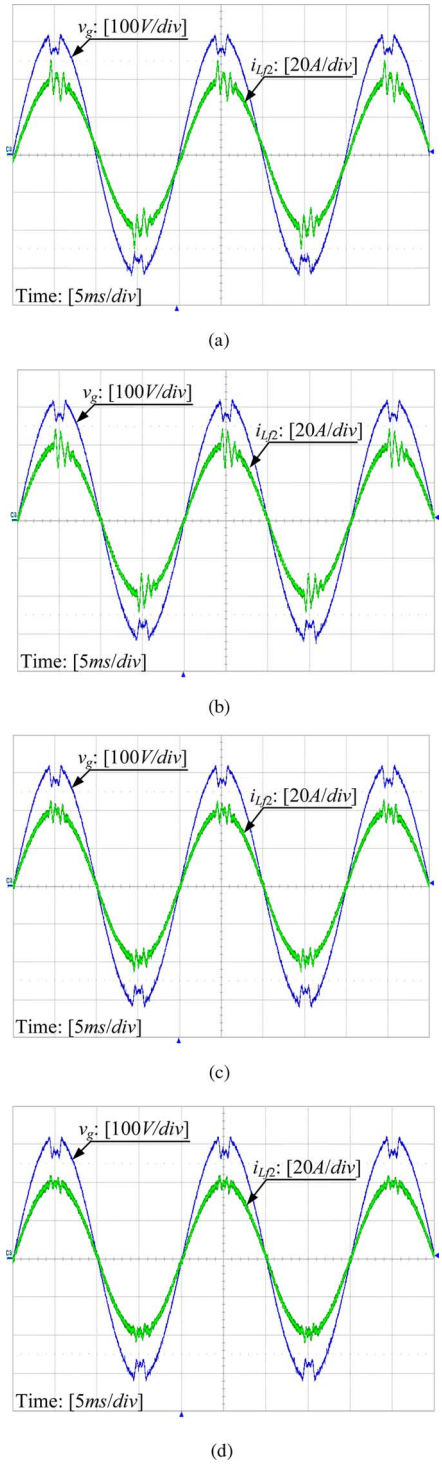

Fig. 15. Experimental waveforms for the four control strategies under voltage dip conditions. (a) Case I. (b) Case II. (c) Case III. (d) Case IV.

The transient response of the grid-connected inverter under the proposed full-feedforward control has been studied, and the

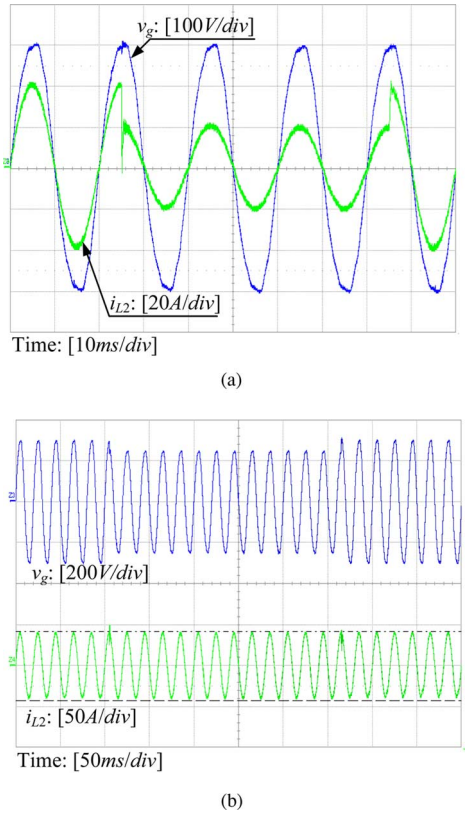

Fig. 16. Measured transient response under (a) step change in $i_{\rm ref}$ and (b) step change in v_g.

results are shown in Fig. 16(a) corresponding to step change of $i_{\rm ref}$. Note that the grid voltage is taken from the real power grid. Here, $i_{\rm ref}$ is stepped up from half load to full load, and *vice versa*. The load changes are intentionally set to occur at the peak of i_{L_2}, which is the worst case. The results show that i_{L_2} is still kept in phase with v_g, with small oscillatory transient observed immediately after the step change of $i_{\rm ref}$. Also, Fig. 16(b) shows the transient response corresponding to step change of v_g with the full-feedforward scheme. Here, v_g is stepped down from 220 to 180 V, and *vice versa*. The v_g changes are again purposely set to occur at the peak of v_g, which is the worst case. Results show that the amplitude of i_{L_2} is kept unchanged, with small oscillatory transient immediately following the step change of v_g.

VII. Conclusion

For the grid-connected inverter with an *LCL* filter, the dual-loop control strategy with feedback of the capacitor and the injected current can damp the resonance effectively, but it cannot attenuate the current distortion resulted from the harmonics in the grid voltage. The traditional solution of applying a feedforward grid voltage can suppress such current distortion, but the result is not satisfactory, especially when the order of the harmonics is high. This paper proposes a full feedforward of grid voltage scheme to suppress the injected current distortion arising from harmonics in the grid voltage. Four cases of control schemes, namely, dual-loop control strategy without feedforward, dual-loop strategy with proportional feedforward of the grid voltage, dual-loop strategy with proportional and derivative feedforward of the grid voltage, and dual-loop strategy with full feedforward of the grid voltage, are compared. Some design guidelines are recommended. Our results show that if the grid voltage contains only the third harmonic, proportional feedforward of the grid voltage is adequate for achieving good suppression of the current distortion. If the grid voltage contains harmonic distortion up to 13th harmonic, proportional and derivative feedforward of the grid voltage is adequate for achieving good suppression of the current distortion. If the grid voltage contains higher harmonic distortion, the full feedforward of the grid voltage becomes necessary. Furthermore, the proposed feedforward scheme has an added merit that it is able to reduce the steady-state error of the injected current significantly even if simple conventional PI regulation is used. The injected current can thus accurately track the reference current for most practical applications.

References

[1] F. Blaabjerg, R. Teodorescu, M. Liserre, and A. V. Timbus, "Overview of control and grid synchronization for distributed power generation systems," *IEEE Trans. Power Electron*, vol. 53, no. 5, pp. 1398–1409, Oct. 2006.

[2] N. Hatziargyriou, H. Asano, R. Iravani, and C. Marnay, "Microgrids," *IEEE Power Energy Mag.*, vol. 5, no. 4, pp. 78–94, Jul./Aug. 2007.

[3] Y. A. R. I. Mohamed and E. F. E. Saadany, "Adaptive decentralized droop controller to preserve power sharing stability of paralleled inverters in distributed generation microgrids," *IEEE Trans. Power Electron.*, vol. 23, no. 6, pp. 2806–2816, Nov. 2008.

[4] H. Kim, T. Yu, and S. Choi, "Indirect current control algorithm for utility interactive inverters in distributed generation systems," *IEEE Trans. Power Electron.*, vol. 23, no. 3, pp. 1342–1347, May 2008.

[5] Y. Sozer and D. A. Torrey, "Modeling and control of utility interactive inverters," *IEEE Trans. Power Electron.*, vol. 24, no. 11, pp. 2475–2483, Nov. 2009.

[6] C. L Chen, Y. Wang, J. S. Lai, Y. S. Lee, and D. Martin, "Design of parallel inverters for smooth mode transfer microgrid applications," *IEEE Trans. Power Electron.*, vol. 25, no. 1, pp. 6–15, Jan. 2010.

[7] T. C. Y. Wang, Z. H. Ye, G. Sinha, and X. M. Yuan, "Output filter design for a grid-interconnected three-phase inverter," in *Proc. IEEE PESC,* 2003, pp. 779–784.

[8] E. Wu and P. W. Lehn, "Digital current control of a voltage source converter with active damping of LCL resonance," *IEEE Trans. Power Electron.*, vol. 21, no. 5, pp. 1364–1373, Sep. 2006.

[9] W. Gullvik, L. Norum, and R. Nilsen, "Active damping of resonance oscillations in LCL-filters based on virtual flux and virtual resistor," in *Proc. EPE,* 2007, pp. 1–10.

[10] M. Liserre, F. Blaabjerg, and S. Hansen, "Design and control of an LCL-filter-based three-phase active rectifier," *IEEE Trans. Ind. Appl.*, vol. 41, no. 5, pp. 1281–1291, Sep./Oct. 2005.

[11] G. Shen, D. Xu, L. Cao, and X. Zhu, "An improved control strategy for grid-connected voltage source inverters with a LCL filter," *IEEE Trans. Power Electron.*, vol. 43, no. 5, pp. 1899–1906, Jul. 2008.

[12] M. Malinowski and S. Bernet, "A simple voltage sensorless active damping scheme for three-phase PWM converters with an LCL-filter," *IEEE Trans. Ind. Electron.*, vol. 5, no. 4, pp. 1876–1880, Apr. 2008.

[13] V. Blasko and V. Kaura, "A novel control to actively damp resonance in input LC filter of a three-phase voltage source converter," *IEEE Trans. Ind. Appl.*, vol. 33, no. 2, pp. 542–550, Mar./Apr. 1997.

[14] E. Twining and D. G. Holmes, "Grid current regulation of a three-phase voltage source inverter with an LCL input filter," *IEEE Trans. Power Electron.*, vol. 18, no. 3, pp. 888–895, May 2003.

[15] M. Liserre, A. D. Aquila, and F. Blaabjerg, "Genetic algorithm-based design of the active damping for an LCL-filter three-phase active rectifier," *IEEE Trans. Power Electron.*, vol. 19, no. 1, pp. 76–86, Jan. 2004.

[16] M. Liserre, R. Teodorescu, and F. Blaabjerg, "Stability of photovoltaic and wind turbine grid-connected inverters for a large set of grid impedance values," *IEEE Trans. Power Electron.*, vol. 21, no. 1, pp. 263–272, Jan. 2006.

[17] F. Liu, Y. Zhou, S. Duan, J. Yin, B. Liu, and F. Liu, "Parameter design of a two-current-loop controller used in a grid-connected inverter system with LCL filter," *IEEE Trans. Ind. Electron.*, vol. 56, no. 11, pp. 4483–4491, Nov. 2009.
[18] K. Jalili and S. Bernet, "Design of LCL filter of active-front-end two-level voltage-source converters," *IEEE Trans. Ind. Electron.*, vol. 56, no. 5, pp. 1674–1689, May 2009.
[19] D. N. Zmood and D. G. Holmes, "Stationary frame current regulation of PWM inverters with zero steady-state error," *IEEE Trans. Power Electron.*, vol. 18, no. 3, pp. 814–822, May 2003.
[20] A. Timbus, M. Liserre, R. Teodorescu, P. Rodriguez, and F. Blaabjerg, "Evaluation of current controller for distributed power generation systems," *IEEE Trans. Power Electron.*, vol. 24, no. 3, pp. 654–664, Mar. 2009.
[21] T. Abeyasekera, C. M. Johnson, D. J. Atkinson, and M. Armstrong, "Suppression of line voltage related distortion in current controlled grid connected inverters," *IEEE Trans. Power Electron.*, vol. 20, no. 6, pp. 1393–1401, Nov. 2005.
[22] S. Y. Park, C. L. Chen, J. S. Lai, and S. R. Moon, "Admittance compensation in current loop control for a grid-tie LCL fuel cell inverter," *IEEE Trans. Power Electron.*, vol. 23, no. 4, pp. 1716–1723, Nov. 2005.
[23] J. Dannehl, F. W. Fuchs, S. Hansen, and P. B. Thogersen, "Investigation of active damping approaches for PI-based current control of grid-connected pulse width modulation converters with LCL filters," *IEEE Trans. Ind. Appl.*, vol. 46, no. 4, pp. 1509–1517, Jul./Aug. 2010.

Xuehua Wang was born in Hubei Province, China, in 1978. He received the B.S. degree in electrical engineering from Nanjing University of Technology, Nanjing, China, in 2001, and the M.S. and Ph.D. degrees in electrical engineering from Nanjing University of Aeronautics and Astronautics, Nanjing, in 2004 and 2008, respectively.

He is currently a Postdoctoral Research Fellow in the College of Electrical and Electronic Engineering, Huazhong University of Science and Technology, Wuhan, China. His research interests include multilevel inverter and renewable energy generation system.

Xinbo Ruan (M'97–SM'02) was born in Hubei Province, China, in 1970. He received the B.S. and Ph.D. degrees in electrical engineering from Nanjing University of Aeronautics and Astronautics (NUAA), Nanjing, China, in 1991 and 1996, respectively.

In 1996, he joined the Faculty of Electrical Engineering Teaching and Research Division, NUAA, where he became a Professor in 2002 at the College of Automation Engineering and has been engaged in teaching and research in the field of power electronics. From August to October 2007, he was a Research Fellow in the Department of Electronics and Information Engineering, Hong Kong Polytechnic University, Hunghom, Hong Kong. Since March 2008, he has been with the College of Electrical and Electronic Engineering, Huazhong University of Science and Technology, Wuhan, China. He has authored or coauthored more than 100 technical papers in journals and conferences and also published three books. His current research interests include soft-switching dc/dc converters, soft-switching inverters, power factor correction converters, modeling the converters, power electronics system integration, and renewable energy generation system.

Dr. Ruan was the recipient of Delta Scholar by the Delta Environment and Education Fund in 2003, and was awarded the Special Appointed Professor of the Chang Jiang Scholars Program, by the Ministry of Education, China, in 2007. He is also the Guest Professor of Beijing Jiaotong University, China, and Hefei University of Technology, China. Since 2005, he has been the Vice President of the China Power Supply Society, and since 2008, he has been the member of the Technical Committee on Renewable Energy Systems within the IEEE Industrial Electronics Society. He is a Senior Member of the IEEE Power Electronics Society and the IEEE Industrial Electronics Society.

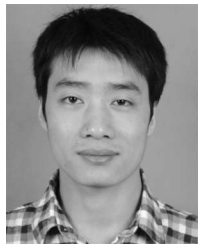

Shangwei Liu was born in Hubei Province, China, in 1983. He received the B.S. degree in electrical engineering from Naval University of Engineering, Wuhan, China, in 2006. He is currently working toward the M.S. degree in electrical engineering in Huazhong University of Science and Technology, Wuhan.

His current research interests include digital control technique and renewable energy generation system.

Chi K. Tse (M'90–SM'97–F'06) received the B.E. degree with first class honors in electrical engineering and the Ph.D. degree from the University of Melbourne, Australia, in 1987 and 1991, respectively.

He is currently the Chair Professor and the Head of Department of Electronic and Information Engineering, Hong Kong Polytechnic University, Hunghom, Hong Kong. He is the author of the books *Linear Circuit Analysis* (London: Addison-Wesley, 1998) and *Complex Behavior of Switching Power Converters* (Boca Raton: CRC Press, 2003), the coauthor of *Chaos-Based Digital Communication Systems* (Heidelberg: Springer-Verlag, 2003), *Digital Communications with Chaos* (London: Elsevier, 2006), *Reconstruction of Chaotic Signals with Applications to Chaos-Based Communications* (Singapore: World Scientific, 2007), and *Sliding Mode Control of Switching Power Converters: Techniques and Implementation* (Roca Raton: CRC Press, 2010), and the coholder of three U.S. patents and two other pending patents. His research interests include complex network applications, power electronics, and chaos-based communications.

Dr. Tse was the recipient of the L.R. East Prize from the Institution of Engineers, Australia, in 1987, the Best Paper Award from IEEE TRANSACTIONS ON POWER ELECTRONICS in 2001 and the Best Paper Award from *International Journal of Circuit Theory and Applications* in 2003. In 2005, he was named an IEEE Distinguished Lecturer. In 2007, he was the recipient of the Distinguished International Research Fellowship by the University of Calgary, Canada. In 2009, he and his coinventors won the Gold Medal with Jury's Commendation at the International Exhibition of Inventions of Geneva, Switzerland, for a novel driving technique for LEDs. In 2010, he was appointed for the Chang Jiang Scholar Chair Professorship by the Ministry of Education of China and the appointment is hosted by Huazhong University of Science and Technology, Wuhan, China. He is currently the Deputy Editor-in-Chief for the *IEEE Circuits and Systems Magazine* and the Editor-in-Chief of IEEE Circuits and Systems Society Newsletter. He was/is an Associate Editor for the IEEE TRANSACTIONS ON CIRCUITS AND SYSTEMS PART I—FUNDAMENTAL THEORY AND APPLICATIONS from 1999 to 2001 and again from 2007 to 2009. He has also been an Associate Editor for the IEEE TRANSACTIONS ON POWER ELECTRONICS since 1999. He is an Associate Editor of the *International Journal of Systems Science*, and also on the Editorial Board of the *International Journal of Circuit Theory and Applications* and *International Journal and Bifurcation and Chaos*. He also served as Guest Editor and Guest Associate Editor for a number of special issues in various journals. He is a Fellow of the Institution of Engineers, Australia.